CO_2 Reduction with Zn Particles in a Packed-Bed Reactor

Peter G. Loutzenhiser, Frank Barthel, and Anastasia Stamatiou
Dept. of Mechanical and Process Engineering, ETH Zurich, Zurich 8092, Switzerland

Aldo Steinfeld
Dept. of Mechanical and Process Engineering, ETH Zurich, Zurich 8092, Switzerland; and Solar Technology Laboratory, Paul Scherrer Institute, Villigen 5232, Switzerland

DOI 10.1002/aic.12460
Published online December 15, 2010 in Wiley Online Library (wileyonlinelibrary.com).

A two-step solar thermochemical cycle for splitting CO_2 with Zn/ZnO redox reactions is considered, consisting of: (1) the endothermic dissociation of ZnO with concentrated solar radiation as the heat source and (2) the non-solar, exothermic, reduction of CO_2 to CO by oxidizing Zn to ZnO; the latter is recycled to the first step. The second step of the cycle is investigated using a packed-bed reactor where micron-sized Zn particles were immobilized in mixtures with submicron-sized ZnO particles. Experimental runs were performed for Zn mass fractions in the range 67–100 wt % and CO_2 concentration in the range 25–100%, yielding Zn-to-ZnO conversions up to 71% because of sintering prevention, as corroborated by SEM analysis. © 2010 American Institute of Chemical Engineers *AIChE J,* 57: 2529–2534, 2011
Keywords: energy, fuels, reactor analysis, surface chemistry/physics

Introduction

A two-step solar thermochemical cycle to reduce CO_2 to CO and O_2 using Zn/ZnO redox reactions was examined in a previous work.[1] The first step is the endothermic dissociation of ZnO to Zn and O_2 using concentrated solar radiation as the energy source of process heat, formulated as:

$$\mathrm{ZnO} \rightarrow \mathrm{Zn} + \frac{1}{2}\mathrm{O_2} \tag{1}$$

and experimentally demonstrated in solar reactors at ~2000 K.[2–7] The second non-solar step is the exothermic reaction of Zn with CO_2, formulated as:

$$\mathrm{Zn} + \mathrm{CO_2} \rightarrow \mathrm{ZnO} + \mathrm{CO} \tag{2}$$

The resulting ZnO is recycled back to the first step, resulting in a net reaction $CO_2 \rightarrow CO + {}^1/_2O_2$. The advantages of the two-step cycle vis-à-vis the direct thermolysis of CO_2 are the lower upper operating temperatures and the elimination of the CO—O_2 separation to avoid their recombination upon cooling. Similar studies for splitting CO_2 using ferrites[8–17] and ceria redox reactions[18] and for splitting H_2O with various metal oxide redox reactions[19] have been performed. This work focuses on the second, non-solar, exothermic step, Eq. 2, which can be decoupled from the solar step and therefore performed continuously at a convenient site, independent of the solar energy availability. Thermogravimetric analyses (TGA) of μm-sized Zn particles reacting with CO_2 and with a mixture of CO_2 and H_2O were performed to ascertain the reaction mechanisms and determine kinetic parameters.[20–22] Two distinct reaction regimes were identified: an initial fast interface-controlled regime that transitioned to a diffusion-controlled regime limited by ion mobility through the ZnO layer. Low Zn conversions to ZnO were obtained due to particle sintering and slow diffusion rates. The reaction of CO_2 with Zn was also studied in an aerosol flow reactor designed for in situ quench of Zn vapor below the saturation temperature to form nanoparticles.[23]

Correspondence concerning this article should be addressed to A. Steinfeld at aldo.steinfeld@ethz.ch.

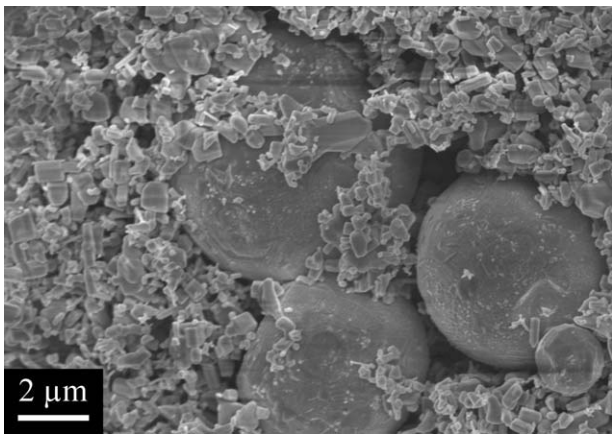

Figure 1. SEM analysis of μm-sized Zn particles immobilized in a packed bed with sub-μm-sized ZnO particles.

This offered high Zn-to-ZnO conversions over short residence times (e.g., up to 88% over 3 s) due to augmented reaction kinetics and heat/mass transfer. However, the reaction primarily occurred heterogeneously outside the aerosol jet flow on surfaces with Zn deposition, making the ZnO recovery, process control, and scale-up problematic.

Given the aforementioned limitations, a new fixed-bed reactor concept was explored with the aim of maximizing both Zn conversions and ZnO recovery while alleviating some of the process technology issues associated with control and scale-up. Various supports were initially examined to immobilize micro-sized Zn particles similar in size to those obtain from the solar ZnO dissociation step[24] and to isolate them for preventing sintering. Example of supports often used in catalytic combustion that provide low pressure drops and high specific surface areas include: honeycomb structures,[25] wire-meshes,[26,27] and highly porous meshes.[28,29] Interestingly, a packed-bed containing a mixture of Zn and ZnO particles offers effective inert support for preventing sintering and—after reaction completion—inherently enables simple and complete recovery of ZnO particles for recycling to the first solar step. This study examines the effects of the mass fraction of Zn in ZnO at different CO_2 concentrations on the overall chemical conversion of Zn to ZnO.

Experimental

Experimentation was performed using a packed-bed of Zn/ZnO particles contained in a 25-mm diameter quartz tube, which was positioned vertically in an electric furnace (Heraeus Ref 4/25, 0.95kW). A type-K thermocouple (TC) located on top of the bed was maintained at 674 K, just below the Zn melting point (692.68 K). The samples were held by a quartz porous disk and heated to a constant temperature in Ar (>99.99% purity). The heights of the reactor bed with 500 mg of Zn for 100, 75, and 67 wt % Zn were 1.0, 1.5, and 2.0 mm, respectively; and with residence times through the packed-bed, determined assuming plugged flow, equal to 39.8, 59.7, and 79.6 ms, respectively. Once quasi-steady conditions were attained, CO_2 (>99.99% purity) was introduced in the system. Flow rates and mixtures of Ar-CO_2 were regulated by two electronic flow controllers (Bronkhorst F-201CV), with a total mass flow rate of 0.3 l_N/min (l_N means liters under normal conditions at 273 K and 1 atm) to prevent particle entrainment. The product gas composition was monitored temporally by gas chromatography (GC, Varian CP-4900 Micro-GC two-channel system, 100 ppm detection limit). The surface morphologies of the samples before and after experimentation were analyzed by scanning electron microscopy (SEM, SmartSEM, Carl Zeiss Supra 55VP). BET specific surface area was measured by N_2 adsorption at 77 K (Micromeritics TriStar 3000).

Zn particles (Sigma-Aldrich, 98+% purity, 7.9-μm mean size) were mixed with ZnO particles (Alpha Aesar, −325 Mesh, 99% purity, 0.22-μm mean size). The ZnO particles were identical to those employed to study ZnO thermolysis in a solar chemical reactor, while the Zn particles were similar in size to products collected from the filter resulting from experimentation to thermolyze ZnO with concentrated solar irradiation.[4–6,30] The initial amount of Zn was 500 mg at Zn mass fractions of 67, 75, and 100 wt %. The composition of reacting flow was 25, 50, and 75% CO_2-Ar and 100% CO_2. An additional experiment was performed with a Zn mass of 2000 mg at 67 Zn wt % and 100% CO_2 to evaluate the impact of increasing the packed-bed thickness. Figure 1 shows the SEM pictures of the reactants, characterized by the μm-sized Zn smooth spherical balls of Zn surrounded by the sub-μm-sized particles of ZnO.

Results and Discussion

A total of 24 experiments were carried out at various Zn mass fractions in Zn/ZnO mixtures and CO_2 concentrations in Ar. Two experiments were performed for each condition for statistical analysis, and an additional experiment was performed to verify results for solid samples with increasing mass. Figure 2 shows the temporal variation of the molar

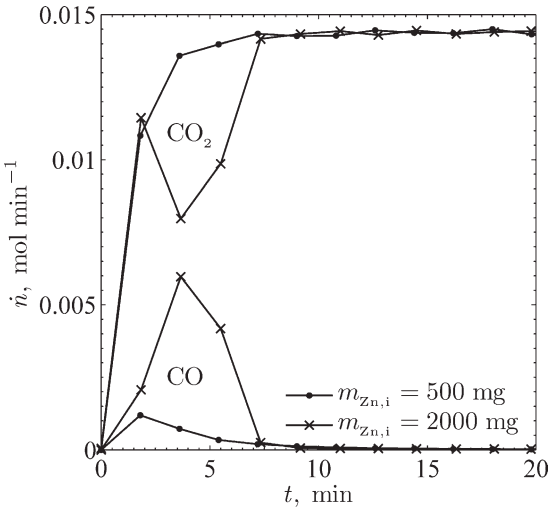

Figure 2. Temporal variation of the molar flow rates of CO_2 and CO in the product gas for a representative run with 67 Zn wt % and 100% CO_2 at 674 K.

The Zn initial mass was 500 mg (dots) and 2000 mg (crosses).

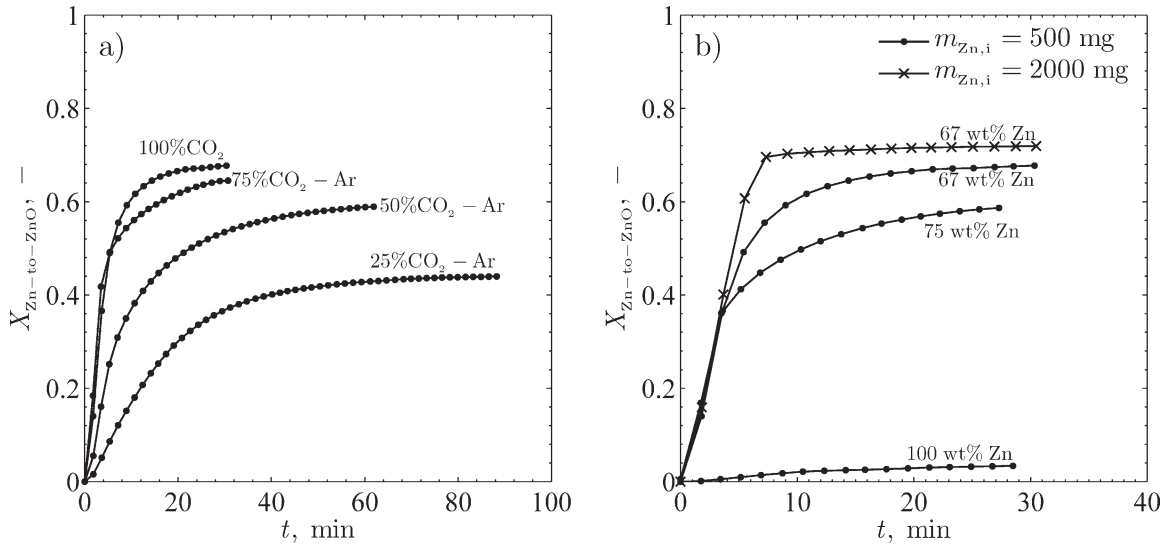

Figure 3. Temporal variation of the conversions of Zn to ZnO for: (a) 67 wt % Zn with 25, 50, and 75% CO2-Ar and 100% CO2 and (b) 100% CO2 with 67, 75, and 100 wt % Zn.

flow rates of CO_2 and CO in the product gas for a representative run with 67 Zn wt % and 100% CO_2 at 674 K and $m_{Zn,i} = 500$ and 2000 mg. A rapid increase in $\dot{n}_{CO_2}$ was observed over the first 5 min as Ar was displaced from the system and CO_2 was rapidly converted to CO by Zn oxidation. $\dot{n}_{CO}$ rapidly increased over the first 4 min and then decreased as the majority of the available Zn was oxidized. After 20 min, CO was no longer detected by GC. The CO evolution was higher for $m_{Zn,i} = 2000$ mg, where the instantaneous conversion of CO_2 to CO peaked at 0.43 compared to 0.26 for $m_{Zn,i} = 500$ mg.

Zn-to-ZnO conversions

The chemical conversion of Zn to ZnO is defined as:

$$X_{Zn-to-ZnO} = \frac{n_{ZnO}}{n_{Zn,i}} = \frac{\sum \dot{n}_{CO} \Delta t}{n_{Zn,i}} \tag{3}$$

where $n_{Zn,i}$ denotes the initial molar amount of Zn, n_{ZnO} denotes the molar amount of ZnO produced, $\dot{n}_{CO}$ is the molar flow rate of CO determined from the GC and mass flow rate measurements assuming ideal gas behavior, and Δt is the time increment between GC measurements. $X_{Zn\text{-}to\text{-}ZnO}$ was calculated over entire experiment until CO was not detectable by the GC. The integrations were performed with average values at the beginning and end of each Δt, resulting in smoothing of the temporal results. Previous TGA[22] with 100 mg of initial Zn have shown that Zn-to-ZnO conversions from thermogravimetry compare well with those determined with lower temporal resolution gas chromatography, which were slightly underestimated. Although thermodynamically favorable, no C is formed.[1,20,23]

Figure 3 shows the temporal variation of $X_{Zn\text{-}to\text{-}ZnO}$ for: (a) 67 wt % Zn reacting with 25, 50, and 75% CO_2-Ar and 100% CO_2 (Figure 3a) and (b) 100% CO_2 reacting with 67, 75, and 100 wt % Zn (Figure 3b), including an additional run with 2000 mg of Zn. The time response of the reactor was equal to ~3 min, which accounts for varying CO_2 and CO sums over the first few minutes of experimentation. All curves are characterized by an initial fast interface-controlled regime followed by a transition to a slower diffusion-controlled regime, as previously observed in thermogravimeter measurements.[20] Reaction rates increase with CO_2 concentration (Figure 3a), consistent with the power rate law, and the overall conversion represents a marked difference between results obtained from TGA.[20] No significant differences were seen for the reaction rates with100% CO_2 (Figure 3b), presumably due to faster kinetics coupled to lower temporal resolution of the gas concentration measurements, especially at the beginning, compared to what is realized in TGA. The run with 2000 mg of Zn has nearly the same reaction rate as those with 500 mg and slightly higher $X_{Zn\text{-}to\text{-}ZnO}$, which is indicative of the potential to scale-up the packed-bed. The slightly higher conversions are believed to be due to longer residence times within the packed bed that promote Zn sublimation and redeposition around ZnO nuclei formed initially, as CO_2 is converted to CO and the concentration decreases across the bed. However, it is expected that when the bed reaches a critical height, the advantages of longer residence times and lower initial, outlet CO_2 concentrations will be offset by additional mass that compresses the particles together and limits the available surface towards the inlet of the packed-bed. Several thin beds in series could bypass this problem. $X_{Zn\text{-}to\text{-}ZnO}$ decreased with the Zn wt %, and significant differences were seen using 100% Zn as $X_{Zn\text{-}to\text{-}ZnO} = 0.03$ for a much slower reaction rate. In the absence of the ZnO supports, the Zn particles sintered, reducing the specific surface area and limiting the availability of adsorption sites and pathways for CO_2 to pass through the packed-bed. The reaction rate was significantly slower as gas diffusion within the bed and ionic diffusion through the ZnO layer became the limiting reaction mechanisms. For all runs with Zn/ZnO mixtures, the ZnO particles were effective in immobilizing the Zn particles and preventing sintering.

Figure 4 shows the $\overline{X}_{Zn\text{-}to\text{-}ZnO}$ with error bars based on individual 95% confidence intervals[31] as a function of %

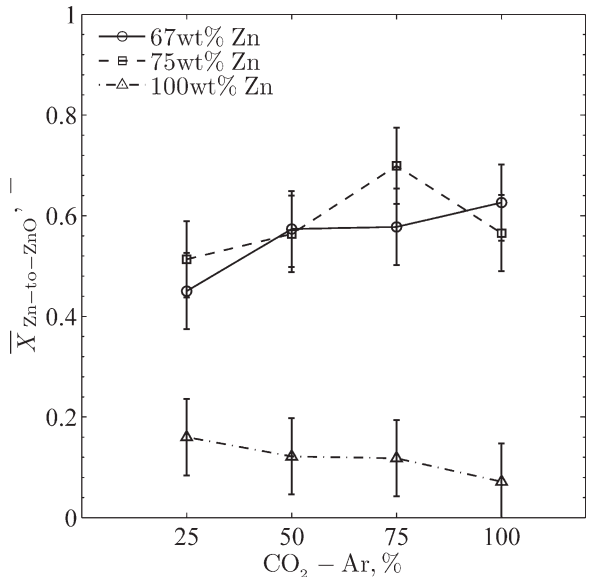

Figure 4. Individual Zn-to-ZnO conversion means with error bars based on individual 95% confidence limits as a function of CO_2 concentration for Zn wt % = 67% (circles), 75% (squares), and 100% (triangles).

CO-Ar for different Zn wt %. The standard error for the means was 0.0348, indicative of small differences of $X_{Zn\text{-}to\text{-}ZnO}$ for runs with the same configurations and fairly reproducible results. Variances are due to heterogeneities in particle sizes and mixing. For 67 and 75 Zn wt %, $X_{Zn\text{-}to\text{-}ZnO}$ increased with CO_2 concentration, reaching a maximum of 71%. For the 75 Zn wt %, $\overline{X}_{Zn\text{-}to\text{-}ZnO}$ peaked at with 75% CO_2-Ar, while for 67 Zn wt %, $\overline{X}_{Zn\text{-}to\text{-}ZnO}$ peaked at 100% CO_2. With 100 Zn wt %, $\overline{X}_{Zn\text{-}to\text{-}ZnO}$ peaked at 25% CO_2-Ar and decreased with increasing CO_2 concentrations, consistent with results from the TGA[20] where resublimation from the gas phase and needle-like structures occurred at lower CO_2 concentrations, and increased sintering and the formation of thick dense ZnO layers occurred at higher CO_2 concentrations.

Table 1. Two-factor Analysis of Variance (Type III) Table Comparing the Effects and Interaction of CO_2 Concentration and Zn wt % on Overall Zn Conversion to ZnO

Source of Variance	SS	df	MS	F	$P > F$
Zn wt %	1.102	2	0.551	227.1	0
CO_2 concentration	0.0246	3	0.0082	3.38	0.0544
Interactions	0.055	6	0.00917	3.78	0.0239
Error	0.0291	12	0.00243		
Total	1.211	23			

Statistical analysis

The individual $\overline{X}_{Zn\text{-}to\text{-}ZnO}$ were compared using a two-factor analysis of variance to identify the effects of Zn wt %, CO_2 and associated interactions.[32] The overall results are provided in Table 1. There is strong evidence to support significant interactions between CO_2 concentration and Zn wt %. However upon closer inspection of the interactions using a Tukey comparisons,[33] only one the individual $\overline{X}_{Zn\text{-}to\text{-}ZnO}$ differences was below a 5% significance level outside of the main effects: the difference between 25% CO_2-Ar at 67 Zn wt % and 75% CO_2-Ar at 75 Zn wt % ($P = 0.0101$), which is moderately significant. Therefore, the main effects, Zn wt % and CO_2 concentration, were then analyzed. There is little evidence to support differences in $\overline{X}_{Zn\text{-}to\text{-}ZnO}$ based on CO_2 concentration and very strong evidence to support differences in $\overline{X}_{Zn\text{-}to\text{-}ZnO}$ based on Zn wt %. Tukey mean comparisons for Zn wt % showed little or no evidence to support differences between 67 and 75 Zn wt % ($P = 0.5565$) and very strong evidence supporting differences between 100 Zn wt % and both 67 ($P < 0.0001$) and 75 ($P < 0.0001$) Zn wt %.

Particle characterization

Figures 5a, b show SEM pictures of solid products from runs with 100 Zn wt % at 25% CO_2-Ar and 100% CO_2, respectively. Given the high temperature and resulting sintering, only a limited amount of the reacted Zn could be scraped from the top of the bed for 100 wt % Zn as much of the reacted sample adhered to the porous disc. Evidence of significant sintering was observed for both samples as the particles formed large conglomerates that limited access of

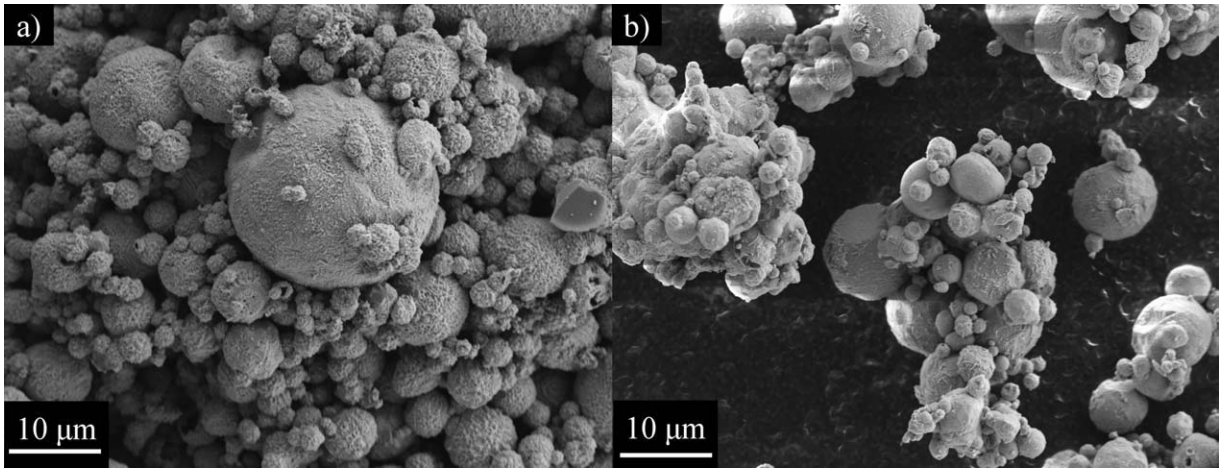

Figure 5. SEM pictures of the solid products from 100 Zn wt % reactions with: (a) 25% CO_2-Ar and (b) 100% CO_2.

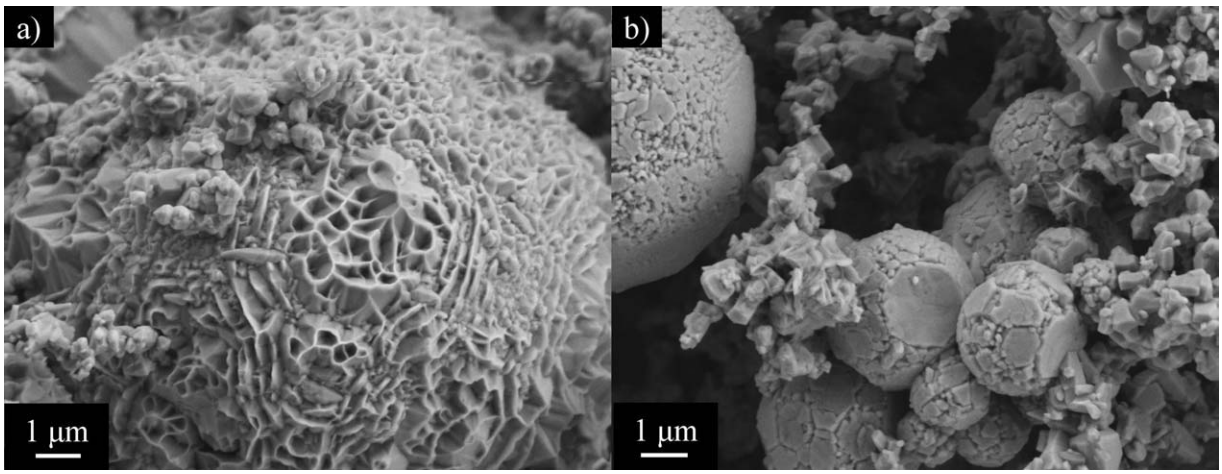

Figure 6. SEM pictures of the solid products from 75 Zn wt % reactions with 100% CO_2 taken from the top (a) and bottom (b) of the packed-bed.

CO_2 to the particle surfaces. The particles, for the most part, remained intact with few holes or cracks forming in the ZnO layer. For the 25% CO_2-Ar case (Figure 5a), the formation of a rough ZnO layer is observed, presumably through Zn sublimation and deposition on already formed ZnO crystals, followed by Zn oxidation with CO_2. For the 100% CO_2 case (Figure 5b), high sintering inhibited Zn sublimation around particles and lead to the formation of a dense ZnO layer that limited CO_2 diffusion through the packed-bed and ionic diffusion through the dense oxide layer.

Figures 6a, b show SEM pictures of solid products from runs with 75 Zn wt % at 100% CO_2 for samples taken from the top and bottom of the packed-bed, respectively. Significantly, less sintering throughout the samples is observed due to the ZnO supports. The samples taken from the top (Figure 6a) show evidence of Zn sublimation and redeposited around ZnO nuclei, as it is apparent from the rough surface ridge-like structures over the entire surface. The samples taken near the bottom (Figure 6b) exhibit a dense and compact ZnO layer as a result of the high CO_2 concentration along with high packing densities. Initial CO_2 concentration gradients through the bed—high at the bottom and low at the top—lead to slower reaction rates at the top. The specific surface areas of the initial Zn and ZnO particles, as measured by BET, were 5.94 and 2.10 m^2/g, respectively. The specific surface areas for solid products with 75% CO_2-Ar was 3.28 m^2/g for 67 Zn wt % and 3.17 m^2/g for 75 Zn wt %.

Summary and Conclusions

The second step of a two-step solar thermochemical cycle for splitting CO_2 has been demonstrated for a packed-bed reactor. The reduction of CO_2 to CO with Zn occurred in a packed-bed consisting of micron-sized Zn particles immobilized in mixtures with submicron-sized ZnO particles. This significantly reduced particle sintering and, consequently, resulted in high $X_{Zn\text{-}to\text{-}ZnO}$. For Zn mass fractions of 67 and 75 wt %, $X_{Zn\text{-}to\text{-}ZnO}$ were from 44 to 71% with lower conversions coupled to lower CO_2 concentrations. For Zn mass fractions of 100%, $X_{Zn\text{-}to\text{-}ZnO}$ were below 20% and decreased with increasing CO_2 concentrations. The maximum $X_{Zn\text{-}to\text{-}ZnO}$ of 71% was obtained at 75 Zn wt % and 75% CO_2-Ar. An additional experiment performed with four times more solid reactants—increasing the bed thickness—garnered similar reaction rates and $X_{Zn\text{-}to\text{-}ZnO}$. Two-factor analysis of variance showed that there were no significant statistical differences due to mass fraction of Zn and CO_2 concentrations and difference between 100 Zn wt % and 67 and 75 Zn wt %. Scanning electron microscopy showed that this was largely due to sintering of Zn particles which limited CO_2 diffusion through the bed and reduced the available surface area.

The packed-bed reactor using Zn/ZnO mixtures yields high Zn-to-ZnO conversions even with 100% CO_2, thereby eliminating inert gas separation. In addition, the use of ZnO particles as supports significantly simplifies solid product recovery for recycling to the first solar step, as both the ZnO supports and products are used. The reactor configuration can be easily linked to ongoing efforts to capture atmospheric CO_2 using with concentrated solar energy,[34] where the captured CO_2 exiting the solar reactor at high temperatures could be fed into the packed-bed reactor to produce CO.

Acknowledgments

This work has been financially supported by the Swiss National Science Foundation, the Swiss Federal Office of Energy, and the Baugarten Foundation. The authors thank R. Kuhn at ETH Zurich and A. Frei at PSI for their technical support with the experimental campaigns.

Notation

$X_{Zn\text{-}to\text{-}ZnO}$ = chemical conversion from Zn to ZnO
m_f = mass fraction
n = molar amount
n_i = initial molar amount
$\dot{n}$ = molar flow rate
t = time
wt % = weight percent

Literature Cited

1. Gálvez ME, Loutzenhiser PG, Hischier I, Steinfeld A. CO_2 splitting via two-step solar thermochemical cycles with Zn/ZnO and FeO/Fe_3O_4 redox reactions—Thermodynamic analysis. *Energy Fuels.* 2008; 22:3544–3550.

2. Haueter P, Möller S, Palumbo R, Steinfeld A. The production of zinc by thermal dissociation of zinc oxide—Solar chemical reactor design. *Solar Energy*. 1999;67:161–167.
3. Müller R, Haeberling P, Palumbo RD. Further advances toward the development of a direct heating solar thermal chemical reactor for the thermal dissociation of ZnO(s). *Solar Energy*. 2006;80:500–511.
4. Schunk L, Haeberling P, Wepf S, Wuillemin D, Meier A, Steinfeld A. A receiver-reactor for the solar thermal dissociation of zinc oxide. *ASME J Solar Energy Eng*. 2008;130:021009-1-6.
5. Schunk L, Steinfeld A. Kinetics of the thermal dissociation of ZnO exposed to concentrated solar irradiation using a solar-driven thermogravimeter in the 1800–2100 K range. *AIChE J*. 2009;55:1497–1504.
6. Schunk L, Lipinski W, Steinfeld A. Heat transfer model of a solar receiver-reactor for the thermal dissociation of ZnO—Experimental validation at 10 kW and scale-up to 1 MW. *Chem Eng J*. 2009;150:502–508.
7. Chambon M, Abanades S, Flamant G. Solar thermal reduction of ZnO and SnO_2: Characterization of the recombination reaction with O_2. *Chem Eng Sci*. 2010;65:3671–3680.
8. Ehrensberger K, Palumbo R, Larson C, Steinfeld A. Production of carbon from carbon dioxide with iron oxides and high-temperature solar energy. *Ind Eng Chem Res*. 1997;36:645–648.
9. Farghali AA, Khedr MH, Abdelkhalek A. Catalytic decomposition of carbondioxide over freshly reduced activated $CuFe_2O_4$ nano-crystals. *J Mater Process Technol*. 2007;181:81–87.
10. Kato H, Kodama M, Tsuji M, Tamaura Y. Decomposition of carbon dioxide to carbon by hydrogen-reduced Ni(II)-bearing ferrite. *J Mater Sci*. 1994;29:5689–5692.
11. Khedr MH, Bahgat M, Nasr MI, Sedeek EK. CO_2 decomposition over freshly reduced nanocrystalline Fe_2O_3. *Colloids Surf A Physicochem Eng Asp*. 2007;302:517–524.
12. Khedr MH, Farghali AA. Microstructure, kinetics and mechanisms of CO_2 catalytic decomposition over freshly reduced nano-crystallite $CuFe_2O_4$ at 400–600°C. *Appl Catal B Environ*. 2005;61:219–226.
13. Ma LY, Chen LS, Chen SY. Study of the CO_2 decomposition over doped Ni-ferrites. *J Phys Chem Solids*. 2007;68:1330–1335.
14. Ma LY, Chen LS, Chen SY. Study on the cycle decomposition of CO_2 over $NiCr_{0.08}Fe_{1.92}O_4$ and the microstructure of products. *Mater Chem Phys*. 2007;105:122–126.
15. Tamaura Y, Tabata M. Complete reduction of carbon dioxide to carbon using cation-excess magnetite. *Nature*. 1990;346:255–256.
16. Zhang CL, Li S, Wang LJ, Wu TH, Peng SY. Studies on the decomposition of carbon dioxide into carbon with oxygen-deficient magnetite I. Preparation, characterization of magnetite, and its activity of decomposing carbon dioxide. *Mater Chem Phys*. 2000;62:44–51.
17. Zhang CL, Li S, Wu TH, Peng SY. Reduction of carbon dioxide into carbon by the active wustite and the mechanism of the reaction. *Mater Chem Phys*. 1999;58:139–145.
18. Chueh WC, Haile SM. Ceria as a thermochemical reaction medium for selectively generating syngas or methane from H_2O and CO_2. *ChemSusChem*. 2009;2:735–739.
19. Steinfeld A. Solar thermochemical production of hydrogen—A review. *Solar Energy*. 2005;78:603–615.
20. Loutzenhiser PG, Gálvez ME, Hischier I, Stamatiou A, Frei A, Steinfeld A. CO_2 splitting via two-step solar thermochemical cycles with Zn/ZnO and FeO/Fe_3O_4 redox reactions II: Kinetic analysis. *Energy Fuels*. 2009;23:2832–2839.
21. Stamatiou A, Loutzenhiser PG, Steinfeld A. Solar syngas production from H_2O and CO_2 via two-step thermochemical cycles based on Zn/ZnO and FeO/Fe_3O_4 redox reactions: Kinetic analysis. *Energy Fuels*. 2010;24:2716–2722.
22. Stamatiou A, Loutzenhiser PG, Steinfeld A. Solar syngas production via H_2O/CO_2-splitting thermochemical cycles with Zn/ZnO and FeO/Fe_3O_4 redox reactions. *Chem Mater*. 2010;22:851–859.
23. Loutzenhiser PG, Galvez ME, Hischier I, Graf A, Steinfeld A. CO_2 splitting in an aerosol reaction via the two-step Zn/ZnO solar thermochemical cycle. *Chem Eng Sci*. 2010;65:1855–1864.
24. Gstöhl D, Brambilla A, Schunk L, Steinfeld A. A quenching apparatus for the gaseous products of the solar thermal dissociation of ZnO. *J Mater Sci*. 2008;43:4729–4736.
25. Yang SK, Choi JS, Lee SH, Chung JS. Development of Al/Al_2O_3 coated wire-mesh honeycombs for catalytic combustion of volatile organic compounds in air. *Ind Eng Chem*. 2004;43:907–912.
26. Ahlström-Silversand AF, Odenbrand CUI. Thermally sprayed wire-mesh catalysts for the purification of flue gases from small-scale combustion of bio-fuel: Catalyst preparation and activity studies. *Appl Catal A Gen*. 1997;153:177–20l.
27. Ahlström-Silversand AF, Odenbrand CUI. Modelling catalytic combustion of carbon monoxide and hydrocarbons over catalytically active wire meshes. *Chem Eng J*. 1999;73:205–216.
28. Richardson JT, Peng Y, Remue D. Properties of ceramic foam catalyst supports: pressure drop. *Appl Catal*. 2000;204:19–32.
29. Richardson JT, Remue D, Hung JK. Properties of ceramic foam catalyst supports: Mass and heat transfer. *Appl Catal*. 2003;250:319–329.
30. Schunk LO. *Solar Thermal Dissociation of Zinc Oxide—Reaction Kinetics, Reactor Design, Experimentation, and Modeling, Diss. ETH No. 18041*.ETH Zurich, Switzerland, 2008.
31. Vardeman SB, Jobe JM. *Basic Engineering Data Collection and Analysis*. Australia: Duxbury Press, 2001.
32. SAS Institute Inc. JMP Version 8.0.2.2. Cary, NC: SAS Institute Inc., 2009.
33. Neter J, Kutner MH, Nachtsheium CJ, Wasserman W. *Applied Linear Statistical Models*, *4th ed*. Boston, MA: WCD McGraw-Hill, 1996.
34. Nikulshina V, Gebald C, Steinfeld A. CO_2 capture from atmospheric air via consecutive CaO-carbonation and $CaCO_3$-calcination cycles in a fluidized-bed solar reactor. *Chem Eng J*. 2009;146:244–248.

Manuscript received Aug. 5, 2010, and revision received Sept. 27, 2010.